Beyond Single-Atom Catalysts: Exploration of Cu Dimer and Trimer for CO_2 Reduction to Methane

Jing Yang[1] , Ximeng Liu[2], Yuan Hao[1], Jianguo Sun[2], Lidao Li[3], Kuan Eng Johnson Goh[4,5,6], Zhi Gen Yu[1], Junmin Xue[2], John Wang[2] and Yong-Wei Zhang[1,*]

[1]Institute of High Performance Computing, A*STAR, Singapore

[2]Department of Materials Science and Engineering, National University of Singapore.

[3]Department of Chemistry, University of Oxford, UK

[4]Institute of Materials Research and Engineering, A*STAR, Singapore.

[5]Department of Physics, National University of Singapore

[6]Division of Physics and Applied Physics, School of Physical and Mathematical Sciences, Nanyang Technological University, 50 Nanyang Avenue 639798, Singapore

Abstract:

We extend the single-atom catalysts (SACs) concept to metal-dimer and trimer catalysts anchored on graphene and explore their characteristic performance in catalyzing CO_2RR into methane using first-principles calculations. In designing the catalyst, we first identify highly energetically stable Cu dimer and trimer atomic configurations in graphene host and then compute the Gibbs free energy changes in the reaction pathway from carbon dioxide to methane. Remarkably, compared to Cu SAC, the limiting potential is 0.60 V for the Cu-

*Corresponding author. email: zhangyw@ihpc.a-star.edu.sg

trimer and 1.22 V for Cu-dimer, which is lower than 1.82 V for SAC. The Cu dimer is suggested to be the optimal choice because it demonstrates reasonably high activity to CO_2RR and high selectivity against HER than SAC. The methodology study suggested that the adsorption term plays the key role in the whole CO_2RR process. The present work points out a new strategy for designing high-performance catalysts beyond single atoms for CO_2RR.

Introduction:

Converting CO_2 into high-value fuels and chemicals using green energy sources under mild reaction conditions is a promising route to address global climate change and energy sustainability issues [1,2]. In this context, there is a pressing need to advance CO_2 utilization and conversion technologies.[3] CO_2 reduction reaction (CO_2RR) by electrochemical methods to fuels and other useful chemicals offers a promising pathway to simultaneously reduce CO_2 emission while providing a source of sustainable energy [4-5].

Great efforts have been made to develop various electrochemical catalysts for CO_2RR recently. Among all the catalysts used for electrochemical CO_2RR to valuable fuels and chemicals, Cu and Cu-based materials stand out as the most promising ones and thus have been extensively studied. A pioneering work reported as early as 1985 showed CH_4 and C_2H_4 as the main products of CO_2RR catalyzed by Cu [6]. However, Cu was shown to exhibit poor selectivity and activity for efficient CO_2 reduction in several pathways [7]. Subsequently, modifications of Cu, for example, through

compounding or alloying, have been extensively studied to enhance its catalytic performance. For example, oxide-derived Cu was shown to efficiently decrease the overpotential and achieve a significantly improved activity of CO_2RR, but the selectivity remained insufficient [8-10]. Sn modified Cu-based alloys could effectively enhance the selectivity of CO_2RR toward CO [11-13]. However, its Faradaic efficiency was found to be low at a low overpotential, resulting in poor energy utilization toward the desired product [14-16].

Single atom catalysts (SACs) have been shown to be a class of effective catalysts for the electrochemical CO_2RR, thus opening a new door for developing low-cost and high-performance catalysts for CO_2RR to fuel and chemical products. These SACs, which are dispersed in a conductive support (predominantly carbon-based materials), are expected to bridge the gap between homogeneous and heterogeneous catalysts and thus behave very differently from their film and nanoparticle counterparts in electrochemical CO_2 reduction [17-19]. For example, Ni single atoms dispersed into graphene nanosheets were reported to exhibit a high CO selectivity of 95% under an overpotential of 550 mV in water, and an excellent stability over 20 hours of continuous electrolysis. In addition, the current density could be scaled up to more than 50 mA cm^{-2} with a CO evolution turnover frequency of 2.1×10^5 hr^{-1}, while maintaining 97% CO selectivity [20]. Fe atoms dispersed in nitrogen-doped graphene were demonstrated as an efficient electrocatalyst for CO_2 reduction to CO. A low reduction overpotential with high Faradic efficiency (FE) up to 80% was reported [21]. Furthermore, Cu single atoms anchored on carbon nanofiber surfaces were able to catalyze CO_2RR to both

methanol with a FE of 44% and CO with a FE of 56% [22].

Building upon the superior catalytic performance of SACs, several interesting questions arise: Can one design an electrochemical catalyst that outperforms SACs? If so, then what might the design be and what is the physical basis behind its improved performance? Here we argue that for different electrochemical reduction reactions, different electron transfer characteristics are required. However, SACs might not be able to offer the right or sufficient electron density for CO_2RR in certain environments, and thus their performance might not be optimal. To supply the right or sufficient electron density, a natural extension is to involve more active atoms in the reactions, such as from the entities of metal dimers, trimers *et al*. Here, we postulate that by introducing such metal mers as electrochemical catalysts, it is possible that we can develop high-performance CO_2RR catalysts that simultaneously possess high activity, selectivity and stability, thus outperforming SACs.

In this study, in addition to Cu SAC on graphene (denoted as 1Cu@Graphene), we design two Cu mer-based catalysts: Cu dimer anchored at graphene (denoted as 2Cu@Graphene), and Cu trimer anchored at graphene (denoted as 3Cu@Graphene). We first examine the stability of all the possible atomic configurations for each of these three catalysts and chose the most stable atomic configuration of each to investigate its possible adsorption sites to identify the most favorable adsorption for the intermediates and compute the Gibbs free energy change (ΔG) along the whole reaction pathway from CO_2 to methane. Remarkably, our calculations show that the Cu dimer and trimer catalysts can significantly outperform the Cu SAC, suggesting a new route to design

electrochemical catalysts. Cu trimer demonstrates the best activity to CO_2RR, however its selectivity to HER is worse. Cu dimer is suggested to be the optimal choice because it shows better activity to CO_2RR than SAC and better selectivity against competing HER. We also analyse the contribution from adsorption, ZPE correction and solvent effect correction, and show that the contribution from adsorption is the most important aspect.

2. Computational Details

All the studies here were performed based on the density functional theory (DFT) with the Perdew-Burke-Ernzerhof functional under the generalized gradient approximation [23-24] for the exchange-correlation interaction, as implemented in the Vienna Ab initio Simulation Package (VASP) [25-26]. A cutoff kinetic energy of 500 eV was applied to expand the electronic wave functions and the projector augmented-wave method was adopted to describe the electron-core interaction. A Gamma centered 3×3×1 k-mesh was used for the structural optimization. To minimize the interaction between adsorbates, a 6×6 graphene unit cell was applied for 1Cu@Graphene and 2Cu@Graphene, while a 7×7 graphene unit cell was applied for 3Cu@Graphene.

The formation energy (E_{form}) of each configuration is defined as the energy required (or released) for a Cu atomic mer (that is, *n*Cu@Graphene, *n* = 1, 2, 3) to be embedded into the defective graphene to form each specific configuration,

$$E_{form} = E_{nCu@Graphene} - E_{defected\ Graphene} - nE_{Cu}, \quad (1)$$

and E_{form} per Cu atom is defined as:

$$E_{form}/Cu = \frac{E_{form}}{n}. \quad (2)$$

Here *n* denotes the number of Cu atoms in an atomic mer. A positive E_{form} indicates

an endothermic reaction while a negative E_{form} indicates an exothermic reaction. This means that the more negative the E_{form} is, the more Cu can be embedded. E_{Cu} is the energy per Cu atom and it can be computed based on the *fcc* Cu metal unit cell.

The adsorption energy (E_{adsorp}) is related to the energy of interaction between the adsorbate and the substrate, which is defined as:

$$E_{adsorp} = E_{adsorpbate-substrate} - E_{substate} - E_{adsorbate}. \quad (3)$$

A positive E_{adsorp} suggests that the adsorption is not thermodynamically favorable while a negative E_{adsorp} suggests that the adsorption process is exothermic. For CO_2RR on *n*Cu@Graphene catalysts, we considered the reaction mechanism of CO_2RR to CH_4 through the adsorbed intermediates *COOH and *CO. The reaction energy (ΔE) is defined as the difference between energy of the products (E_P) and energy of the reactants (E_R):

$$\Delta E = E_P - E_R. \quad (4)$$

The Gibbs free energy change (ΔG) at each electrochemical step involving a proton-electron transfer was computed based on computational hydrogen electrode (CHE) model, in which the free energy of ($H^+ + e^-$) equals to $\frac{1}{2}H_2(g)$ for standard hydrogen electrode (SHE) [27]. So the ΔG of each reaction step is defined as:

$$\Delta G = \Delta E_{adsorp} - \Delta E_{ZPE} - T\Delta S \quad (5)$$

where ΔE_{adsorp} is the adsorption energy differences between the product adsorbate and reactant adsorbate, ΔE_{ZPE} is the difference in zero-point energy, T is the temperature (300 K) and ΔS is the entropy difference between the adsorbed adsorbate and non-adsorbed gas-phase adsorbate. Both ΔE and ΔG describe the energy needed

or released for a reaction to occur. It is understood that the higher the ΔE (or ΔG) is, the more energy is needed for a reaction to take place. The limiting potential (U_e) is defined as the applied potential required to eliminate the energy barrier of the rate-limiting step. Herein, it is an indicator of the catalytic reactivity where a smallerU_e value indicates a faster CO_2RR. In the computational CHE model, the U_e value is determined by:

$$U_e = {}^{\Delta G}/_{e} \tag{6}$$

Here, the ΔG is the free energy of the potential-limiting step. To better mimic the real experiments, solvation effects have been included by using an implicit model [28].

3. Results and Discussions

Graphene, a semimetal, is a promising electrode for CO_2RR. By controlling the electron/ion irradiation intensity, it is feasible to create certain types of point defects, for example, single C vacancies (SVs), double C vacancies (DVs), triple C vacancies (TVs), quadruple C vacancies (QVs), *et al.* in monolayer graphene. These different atomic defect configurations have been demonstrated to host different types and numbers of foreign metal atoms [29]. To find out the most stable atomic configurations of Cu monomer, Cu dimer and Cu trimer embedded in graphene, we carefully examine all the possible atomic configurations as shown in Figure 1 by using DFT calculations. The calculated formation energies are listed in Table 1. Based on the computed formation energies, we map out the most energetically favorable configurations.

3.1 Cu-mers embedded in graphene

When a Cu monomer is embedded at SV and DV sites of graphene (as shown in Figure 1), the formation energies are found to be -1.71 eV and -5.20 eV (Table 1),

respectively. Our result is consistent with previous finding that a Cu monomer at DV site of graphene was more stable than at SV site [30]. Here, a Cu monomer at DV site of graphene is selected as the model for 1Cu@Graphene configuration (Figure 1b). For a Cu dimer, we have carefully examined six possible configurations, as shown in Figure 1. We also notice that when a Cu dimer decorates at DV site (as shown in Figure 1c), the distance between the neighboring Cu atoms is only 1.68 Å, which is much shorter than the typical Cu-Cu bond length of 2.34 Å in Cu metal. Such a short distance may suggest strong repulsion between them, leading to structural instability. This analysis is in line with our calculated formation energy of 0.66 eV per model, suggesting that the process is endothermic and thus unfavorable. There are three possible TV sites and 2 possible QV sites for Cu dimer as shown in Figure 1. Our computed results show that all these embedding processes are exothermic. In particular, a Cu dimer prefers the QV site with the largest formation energy (-5.89 eV per Cu). Hence, we select this configuration as the model for 2Cu@Graphene (Figure 1g). It is noted that this configuration is in line with the previous finding for a bi-metal mer in carbon-based materials [31]. For a Cu trimer, we have examined different atomic configurations, as shown in Figure 1 and Table 1. Our calculations show that it prefers a sextuple C vacancy site and adopts a linear configuration as shown in Figure 1i. Other atomic configurations with more C vacancies are also examined and found that increasing C vacancies is unable to enhance the stability of the Cu trimer, as evidenced by the calculated formation energies summarized in Table 1. Hence, this linear configuration is adopted for 3Cu@Graphene (Figure 1i).

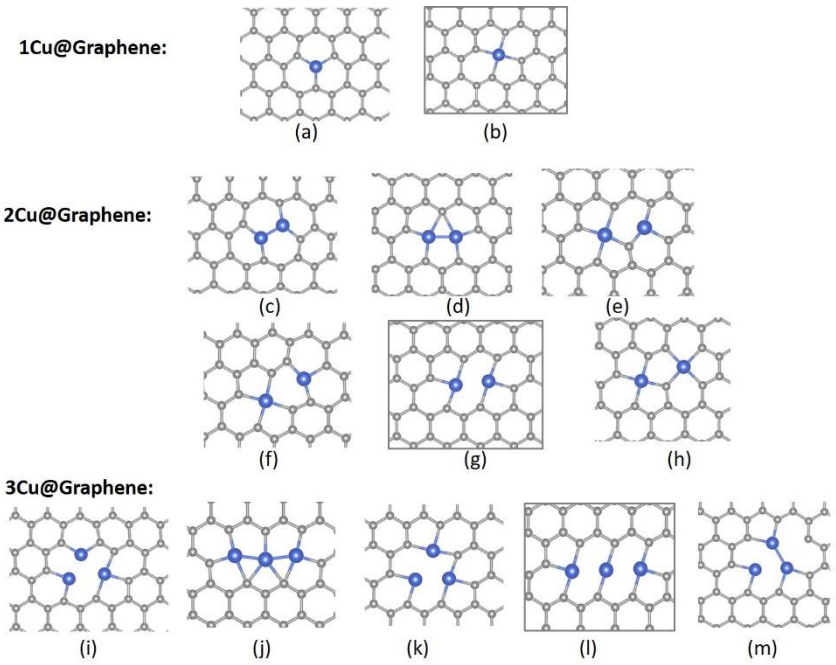

Figure 1. All possible geometries for 1Cu@Graphene, 2Cu@Graphene and 3Cu@Graphene. The one with a black box is adopted as the final model on the basis of its highest formation energy. The grey and blue spheres correspond to carbon and copper atoms, respectively.

Table 1 Formation energy (E_{form}) for each possible geometry of the Cu mer catalysts (in eV). The structure for each possible geometry can be found in Figure 1.

	Geometry	Label	E_{form} /Cu (eV)
1Cu@Graphene	1C missing	a	-1.71
	2C missing	b	-5.20
2Cu@Graphene	2C missing	c	0.33
	3C missing	d	-3.86
		e	-2.55
		f	-4.30
	4C missing	g	-5.89
		h	-4.05
3Cu@Graphene	5C missing	i	-4.13
		j	-5.16
	6C missing	k	-5.69
		l	-6.16
	7C missing	m	-5.38

3.2 Adsorption of intermediates

In the previous section, we have identified the most energetically stable atomic

configurations for each of the three catalysts. Now we would like to examine the adsorptions of all possible intermediates on all possible adsorption sites of each of the three catalysts. It is well-known that adsorption is the first and one of the foremost processes in surface reactions. According to the Sabatier principle, one of the most important guiding rules in heterogeneous catalysis, the adsorption of a reactant on an ideal catalyst should be strong enough so that the surface reaction can take place but not so strong so that the reaction product can desorb [32]. So first and foremost, we explicitly examine the adsorption of all the intermediates, that is, *CO_2, *COOH, *CO, *CHO, *CHOH, *CH, *CH_2, *CH_3 and *H (here, the * indicates adsorption), which are involved in the CO_2RR to CH_4. All the calculated adsorption energies are summarized in Table 2.

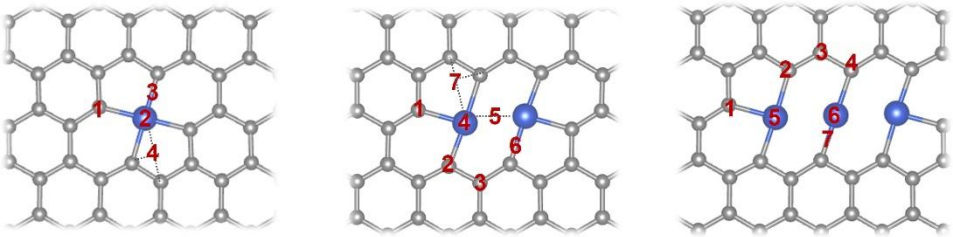

Figure 2. All possible adsorption sites on top of 1Cu@Graphene, 2Cu@Graphene and 3Cu@Graphene, including C-top, Cu-top, bridge and hollow sites. The grey and blue spheres correspond to carbon and copper atoms, respectively.

Adsorption on 1Cu@Graphene: For the 1Cu@Graphene configuration (Figure 1b), we consider four possible adsorption sites on 1Cu@Graphene: The C top site (#1), the Cu top site (#2), the bridge site between the Cu and the C (#3) and the hollow site between Cu-C-C in the five-member ring (#4) as shown in Figure 2a. The most favorable adsorption energies of all intermediates on 1Cu@Graphene are summarized in Table 2. CO_2 adsorbs weakly on 1Cu@Graphene with an E_{adsorp} of -0.03 eV.

Similar weak CO_2 adsorption is also reported on other 2D materials, such as graphene, MoS_2 and stanene [33-35]. It is seen that *COOH prefers to adsorb on the C top site (#1) with an adsorption energy of -2.41 eV. *CO prefers the Cu top site (#2) with a weak physical adsorption of -0.12 eV. While the adsorption energy of on various Cu surface is reported to be around -0.5 eV [36], The difference of the adsorption between 1Cu@Graphene and Cu surface suggests that 1Cu@Graphene plays different role with traditional Cu which catalyzing CO_2RR. *CHO and *CHOH prefer to adsorb on to the C top site (#1) with high chemical binding energies of -2.05 eV and -2.79 eV, respectively. *CH prefers the hollow site (#4), at which it bonds with Cu-C-C to form a tetrahedron geometry with E_{adsorp} of -3.97 eV. *CH_2 prefers the bridge site (#3) while *H and *CH_3 prefer the C top site (#1), all three with high chemical bonding energies (-4.43, -4.40, and -2.66 eV, respectively).

Adsorption on 2Cu@Graphene: For the 2Cu@Graphene configuration (Figure 1g), with one more Cu atom involved, we consider seven possible adsorption sites (#1-#7), as shown in Figure 2b. The most favorable adsorption energies of all intermediates on 2Cu@Graphene are summarized in Table 2. CO_2 adsorbs weakly on 2Cu@Graphene with E_{adsorp} of -0.02 eV. *COOH prefers the C site (#2) with a strong chemical bonding energy of -2.13 eV. Although the most favorable site on 2Cu@Graphene is similarly on a carbon, as with 1Cu@Graphene, their different adsorption energies (-2.13 eV and -2.41 eV for 1Cu and 2Cu@Graphene, respectively) indicate that Cu monomer and Cu dimer have different effects on the neighboring C atoms. *CO prefers the Cu top site (#4) with a weak adsorption energy of only -0.12 eV. *CHO, *CHOH, *CH_3 and *H all prefer the C top site (#2), all with strong chemical adsorptions (E_{adsorp}= -2.39, -3.67, -2.71 and -3.90 eV, respectively). *CH prefers the hollow site

(#7), while *CH_2 prefers the C-Cu bridge site (#6), both with strong adsorption energies (E_{adsorp}=-5.87 eV and -4.52 eV, respectively).

Adsorption on 3Cu@Graphene: For the 3Cu@Graphene configuration (Figure 1i), we also consider seven possible adsorption sites (#1-#7), as shown in Figure 2c for adsorption analysis. The most favorable adsorption energies of all intermediates on 3Cu@Graphene are summarized in Table 2. CO_2 adsorbs weakly on 3Cu@Graphene with E_{adsorp} of -0.02 eV. It is seen that CO prefers to adsorb on the top Cu site (#6), which is the same as on 1Cu@Graphene and 2Cu@Graphene, with a slightly lower adsorption energy of -0.36 eV. The C top site (#4) is preferred by *COOH, *CHO, *CHOH, *CH_3 and *H, all with high chemical adsorption energies (E_{adsorp}= -2.41, -2.58. -2.94, -2.64 and -2.01 eV, respectively). Both *CH and *CH_2 prefer the bridge site (#7) with the adsorption energies of -5.95 eV and -4.78 eV, respectively.

Table 2 The most favorable adsorption energies of all intermediates on 1Cu@Graphene, 2Cu@Graphene and 3Cu@Graphene (in eV).

intermediate	1Cu@Graphene	2Cu@Graphene	3Cu@Graphene
COOH	-2.41	-2.13	-2.41
CO	-0.12	-0.12	-0.36
CHO	-2.05	-2.39	-2.58
CHOH	-2.79	-3.67	-2.94
CH	-4.43	-5.87	-5.95
CH_2	-4.40	-4.52	-4.78
CH_3	-2.66	-2.71	-2.64
CH_4	0.01	-0.01	0.00
H	-3.97	-3.90	-2.01

3.3 Gibbs free energy diagram of the reaction pathway

The CO_2 reduction to CH_4 on Cu crystal surfaces have been extensively studied

using DFT calculations [37-38]. These studies generally suggest a reaction pathway with identical reaction intermediates from CO to CH_4 on both stepped and flat copper crystal surfaces as listed in the left column of Table 3, in which $*CO_2$ is reduced to CH_4 via a series of proton−electron transfers through intermediates of *CHO, *CHOH, *CH, $*CH_2$, and $*CH_3$. We therefore adopt this reaction pathway to examine the reaction energy landscapes of our designed Cu-mer catalysts.

Table 3. ΔG (in eV) of each reaction step for CO_2RR to CH_4 on 1Cu@Graphene, 2Cu@Graphene and 3Cu@Graphene.

Reaction Step	1Cu@Graphene	2Cu@Graphene	3Cu@Graphene
$*CO_2+H = *COOH$	-0.06	0.22	-0.08
$*COOH+H= *CO + H_2O$	0.83	0.54	0.60
$*CO+H = *CHO$	-0.62	-1.01	-0.35
$*CHO+H = *CHOH$	-0.55	-1.01	-0.76
$*CHOH + *H = *CH + H_2O$	1.82	1.22	0.41
$*CH + H = *CH_2$	-2.45	-1.12	-1.28
$*CH_2 + H = *CH_3$	-1.12	-1.06	-0.68
$*CH_3 + H = *CH4$	-0.47	-0.39	-0.48

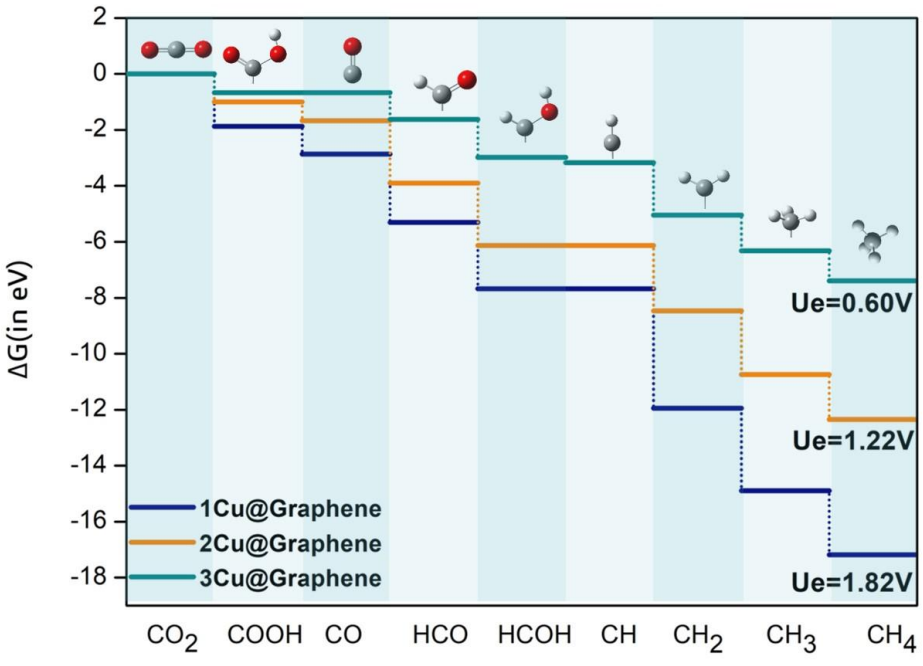

Figure 3. The Gibbs free energy diagram along the reaction pathway for CO_2RR to CH_4 on 1Cu@Graphene (navy), 2Cu@Graphene (orange) and 3Cu@Graphene (green) under their limiting potential (U_e).

Reaction pathway on 1Cu@Graphene: The Gibbs free energy change (ΔG) for each reaction step along the reaction pathway catalyzed by 1Cu@Graphene is given in the second column of Table 3 and navy line of Figure 3 (under U_e). It is seen that under acidic condition, the ΔG associated with the reduction of *CO_2 to *COOH is slightly thermodynamically favorable with a ΔG of -0.06 eV. With this step, the weakly adsorbed *CO_2 ($E_{adsorp} = -0.03\ eV$) was fixed on to the surface in the form of *COOH ($E_{adsorp} = -2.41\ eV$). The reaction from *COOH to *CO is endothermic by 0.83 eV. Although the protonation of *CO to *CHO was widely reported as the rate limiting step for CO_2RR to CH_4 on Cu crystal surfaces [37-38], it is surprising that this reaction step is exothermic by -0.62 eV on 1Cu@Graphene, which indicates that the Cu SAC performs differently from Cu crystal surfaces. The *CHO then releases another -0.55 eV to form *CHOH. However, *CHOH requires as high as 1.82 eV to form *CH. The *CH then undergoes a stepwise spontaneous protonation to *CH_2 (ΔG = -2.45 eV), *CH_3 (ΔG = -1.12 eV) and *CH_4 (ΔG = -0.47 eV). Among all these steps, the reduction of *CHOH to *CH possesses the highest thermodynamics energy barrier (ΔG = +1.82 eV) and is considered the rate-limiting step for CO_2RR to CH_4 on 1Cu@Graphene. Herein, the DFT calculated limiting potential U_e is 1.82 V for 1Cu@Graphene to catalyze CO_2RR to CH_4.

Reaction pathway on 2Cu@Graphene: The value of ΔG for each reaction step along the reaction pathway catalyzed by 2Cu@Graphene is given in the third column of Table 3 and orange line of Figure 3 (under U_e). It is seen that the 2Cu@Graphene performs differently from its 1Cu@Graphene counterpart. The ΔG for *CO_2 protonation to

*COOH is found to be 0.22 eV, which is higher than that on 1Cu@Graphene. Then *COOH requires another 0.54 eV to produce *CO and H_2O. *CO undergoes a spontaneously exothermic reaction to *CHO and *CHOH (ΔG = -1.01 eV and -1.01 eV, respectively). *CHOH needs 1.22 eV to produce *CH. Then, *CH undergoes a stepwise spontaneous protonation to CH_4 (ΔG = -1.12 eV, -1.06 eV and -0.39 eV, respectively). Similar to 1Cu@Grapehene, the C-H bond breaking of *CHOH is the rate-limiting step (ΔG = 1.22 eV). Herein, the DFT calculated limiting potential U_e is 1.22 V for 2Cu@Graphene to catalyze CO_2RR to CH_4. As summarized in Figure 3 and Table 3, the 2Cu@Graphene performs differently from 1Cu@Grapehene due to the ΔG difference in specific reaction steps along the reaction pathway. However, since the U_e on 2Cu@Grapehene is much lower than that on 1Cu@Grapehene (1.22 V *vs* 1.82 V), it is expected that 2Cu@Graphene (orange lines) will outperform 1Cu@Graphene (navy lines) for CO_2RR to CH_4. It is noted that similar Cu dimers with a high activity to CO_2RR were detected in experiments before [39]. It was reported a catalyst that featured two adjacent copper atoms that worked together to promote CO_2 activation, which resulted in a Faradaic efficiency for CO generation up to 92%, and a largely suppressed competing hydrogen evolution reaction [39].

Reaction pathway on 3Cu@Graphene: We have also studied the CO_2RR reaction pathway to CH_4 catalyzed by 3Cu@Graphene. The value of ΔG for each reaction step along the reaction pathway is given in the last column of Table 3 and green line of Figure 3 (under U_e). The ΔG for *CO_2 protonation to *COOH is found to be slightly exothermic by -0.08 eV, which is lower than those on 1Cu@Graphene and 2Cu@Graphene. Then, *COOH requires another 0.60 eV to produce *CO and H_2O. *CO is further reduced to *CHO and gives out -0.35 eV of energy. *CHO is further

protonated, with an exothermic ΔG of -0.76 eV to form *CHOH. *CHOH needs an extra 0.41 eV to produce *CH and H_2O. *CH subsequently undergoes a stepwise spontaneous protonation via *CH_2 and *CH_3 to the final product of CH_4. For 3Cu@Grapehene, the O-H bond breaking of *COOH is the rate-limiting step with a thermodynamic energy barrier of 0.60 eV. Herein, the DFT calculated limiting potential U_e is 0.60 V for 3Cu@Graphene to catalyze CO_2RR to CH_4. Among all three catalysts, both 3Cu@Graphene and 2Cu@Graphene show an improved activity compared with 1Cu@Graphene. Evidently, 3Cu@Graphene (the green lines of Figure 3 and the last column of Table 3) possesses the lowest U_e (0.60 V vs 1.22 V of 2Cu@Graphene and 1.82 V of 1Cu@Graphene), which suggests that it has the best activity for CO_2RR to CH_4.

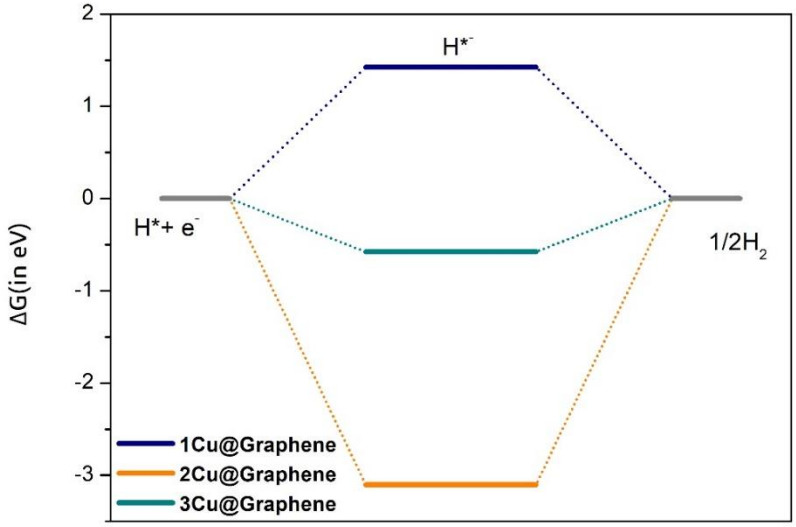

Figure 4. The Gibbs free energy diagram of HER on 1Cu@Graphene (navy), 2Cu@Graphene (orange) and 3Cu@Graphene (green).

Catalytic performance: CO is often considered as being responsible for electrode poisoning due to its strong adsorption on to the electrode surface. For CO_2RR to CH_4 on top of Cu crystal surfaces, regardless flat or stepped, the reduction of *CO is well

accepted as the rate-limiting step [37-38]. Surprisingly, CO adsorbs only weakly on 1Cu@Graphene, 2Cu@Graphene and 3Cu@Graphene (with an absorption energy of -0.12, -0.12 and -0.36 eV, respectively, as shown in Table 2). In addition, the reduction of *CO is exothermic on all three catalysts. This once again shows that atomic mer catalysts present a unique character distinctively different from their Cu crystal surface, thus promising for high-performance catalysis. Hydrogen evolution reaction (HER) is often regarded as a competing reaction with CO_2RR and thus may decrease CO_2RR selectivity and efficiency [40]. The competition between CO_2RR and HER is another concern when designing highly efficient catalyst. Herein, we also compared the performance of these three catalysts on HER, and the relative Gibbs free energy diagrams are shown in Figure 4. Same as the SAC, 1Cu@Graphene shows a low activity (a high selectivity) to HER with ΔG = 1.42 eV. 2Cu@Graphene shows an even lower activity (a higher selectivity) to HER with ΔG = -3.10 eV. Interestingly, 3Cu@Graphene shows a higher activity (a poorer selectivity) to HER with ΔG = -0.58 eV. From the discussion above, we can see that although 3Cu@Graphene shows the best activity to CO_2RR among these three catalysts, it also shows the best activity to HER. As a result, 3Cu@Graphene may not be a good choice because of its poor selectivity against HER. On the other hand, 2Cu@Graphene may be an optimal choice as it shows a reasonably good activity to CO_2RR and a high selectivity against competing HER. 3Cu@Graphene is promising if its poor selectivity against HER can be addressed.

Evaluation of methodology: To have a better understanding on which part of Gibbs energy plays the key role in the whole CO_2RR process, we systematically examined the individual contribution from adsorption, ZPE correction and solvent effect. We also

calculated the reaction energy for each reaction step. All the data are summarized in Figure 5. It is seen that compared to ΔG inclusive of all the three parts (Figure 5(a)), the ΔG without ZPE correction and solvent effect correction (Figure 5(b)) or without the solvent correction (Figure 5(c)) only shifts the energy level of each reaction step but without altering the main trend, that is, the activity for CO_2RR to CH_4 follows the sequence of 3Cu@Graphene > 2Cu@Graphene > 1Cu@Graphene. This signifies that the absorption energy plays the key role in the CO_2RR process. Figure 5(d) shows the reaction energy for each reaction step. It is seen that from a thermodynamic perspective, 3Cu@Graphene is expected to deliver the best performance and 1Cu@Graphene the worst. This conclusion is exactly the same as what we have drawn from the Gibbs free energy calculation without ZPE and solvent effect corrections. In addition, both methods suggest the same rate-limiting step. Finally, we would like to emphasize that since the adsorption plays the key role in the whole CO_2RR process, it should be modelled properly in order to ensure a high accuracy.

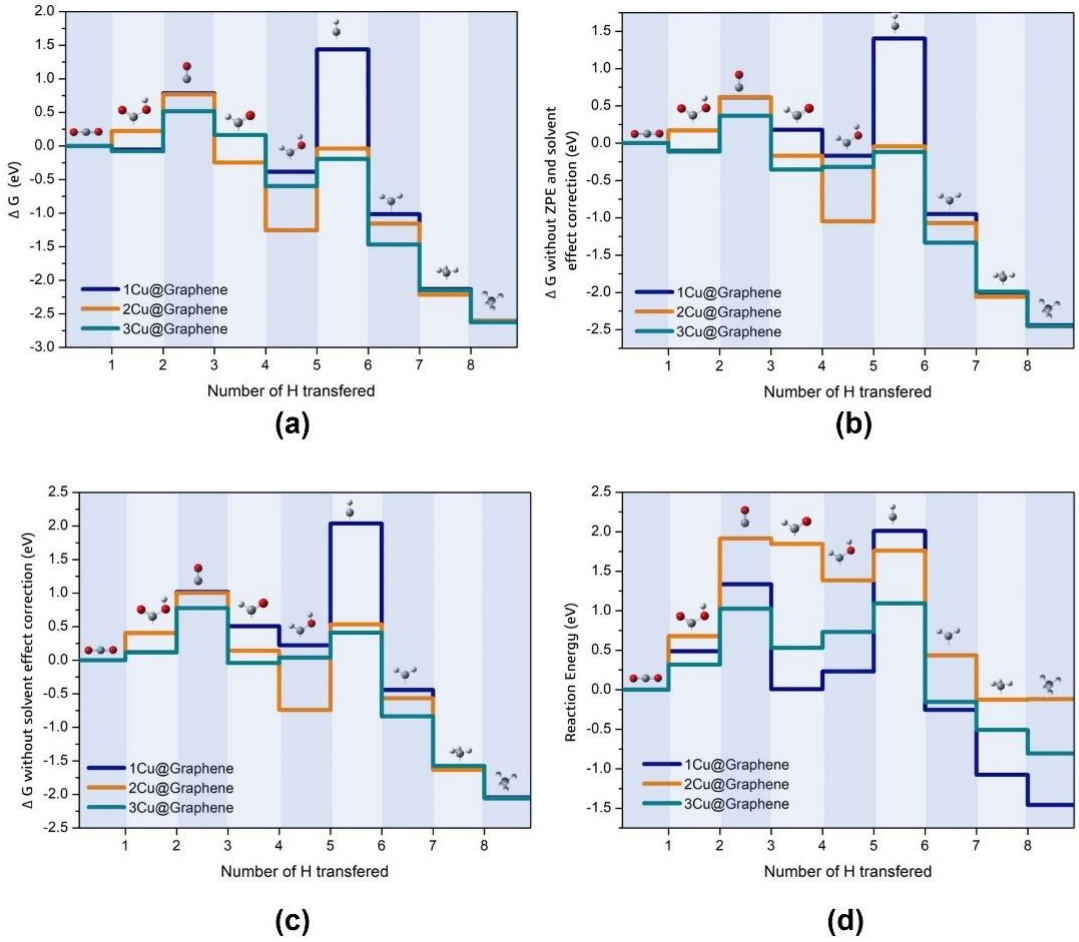

Figure 5. (a) Gibbs free energy inclusive of contributions from all three parts, (b) Gibbs free energy without ZPE and solvent effect corrections, (c) Gibbs free energy without solvent effect correction and (d) reaction energy diagrams along the reaction pathway for CO_2RR to CH_4. 1Cu@Graphene is donated in navy, 2Cu@Graphene in orange and 3Cu@Graphene in green.

4. Conclusion

Going beyond the recently established SACs framework, we have designed Cu dimer and Cu trimer atomic configurations embedded in graphene, and investigated their catalytic performance for CO_2RR to CH_4 by means of DFT calculations. Firstly, we have constructed all the possible atomic models for the 1Cu@Graphene, 2Cu@Graphene and 3Cu@Graphene and screened all possible models to identify the most energetically favorable configurations. Then, we have examined the adsorptions of all the known reaction intermediates from CO_2RR to CH_4 and obtained the most favorable adsorption energies of all the intermediates on the three catalysts. Finally, we

analyzed the Gibbs free energy landscapes of the reaction pathway based on the most favorable adsorption of the reactants and products. For the 1Cu@Graphene, the rate-limiting step is the O-H bond breaking of *CHOH with a U_e of 1.82 V. For the 2Cu@Graphene, the rate-limiting step is the O-H bond breaking of *CHOH with a U_e of 1.22 V. For the 3Cu@Graphene, it effectively lowers the thermodynamic energy barrier of the O-H bond breaking of *CHOH, which results in a much better catalytic activity. The O-H bond breaking of *COOH has instead become the rate-limiting step with a U_e of 0.60 V, clearly outperforming both 1Cu@Graphene and 2Cu@Graphene. However, 3Cu@Graphene also shows the best activity (the poorest selectivity) to HER. As a result, 2Cu@Graphene is expected to be an optimal catalyst because it shows a reasonably good activity to CO_2RR and a high selectivity towards HER. 3Cu@Graphene is a promising candidate if its poor selectivity against HER can be addressed. In addition, we also compared different methodologies and suggested that the adsorption term plays the key role in the whole CO_2RR process, hence it is the most important part in all the calculations and thus should be modelled properly so as to achieve a high accuracy. Our work here unveils a feasible route to design new electrocatalysts with high activity, selectivity and stability for CO_2RR to valuable commodities and chemicals, and presents a useful reference for further experimentation.

Acknowledgement

This work was supported by the National Research Foundation, Singapore under Award No. NRF-CRP24-2020-0002, and Singapore A*STAR SERC CRF Award. The use of computing resources at the A*STAR Computational Centre and National Supercomputer Centre, Singapore is gratefully acknowledged. K.E.J.G.acknowledges

support from Agency for Science, Technology and Research (#21709), and from a Singapore National Research Foundation Grant (CRP21-2018-0001).

References:

(1) Lindsey, R. Climate Change: Atmospheric Carbon Dioxide. https://www.climate.gov/.

(2) Appel, A. M.; Bercaw, J. E.; Bocarsly, A. B.; Dobbek, H.; DuBois, D. L.; Dupuis, M.; Ferry, J. G.; Fujita, E.; Hille, R.; Kenis, P. J. A.; Kerfeld, C. A.; Morris, R. H.; Peden, C. H. F.; Portis, A. R.; Ragsdale, S. W.; Rauchfuss, T. B.; Reek, J. N. H.; Seefeldt, L. C.; Thauer, R. K.; Waldrop, G. L., Frontiers, Opportunities, and Challenges in Biochemical and Chemical Catalysis of CO_2 Fixation. Chem. Rev. 113 (2013) 6621-6658.

(3) Nitopi, S.; Bertheussen, E.; Scott, S. B.; Liu, X.; Engstfeld, A. K.; Horch, S.; Seger, B.; Stephens, I. E. L.; Chan, K.; Hahn, C.; Nørskov, J. K.; Jaramillo, T. F.; Chorkendorff, I., Progress and Perspectives of Electrochemical CO_2 Reduction on Copper in Aqueous Electrolyte. Chem. Rev. 119 (2019) 7610-7672.

(4) Yan, Z.; Hitt, J. L.; Turner, J. A.; Mallouk, T. E., Renewable Electricity Storage Using Electrolysis. Proc.Nati. Acad.Sci. 117 (2020) 12558-12563.

(5) De Luna, P.; Hahn, C.; Higgins, D.; Jaffer, S. A.; Jaramillo, T. F.; Sargent, E. H., What Would It Take for Renewably Powered Electrosynthesis to Displace Petrochemical Processes? Science 364 (2019) eaav3506.

(6) Yoshio, H.; Katsuhei, K.; Shin, S., Production of CO and CH_4 in Electrochemical Reduction of CO_2 at Metal Electrodes in Aqueous Hydrogencarbonate Solution. Chem. Lett. 14 (1985) 1695-1698.

(7) Tao, Z.; Wu, Z.; Wu, Y.; Wang, H., Activating Copper for Electrocatalytic CO_2 Reduction to Formate Via Molecular Interactions. ACS Catal. (2020) 9271-9275.

(8) Li, C. W.; Kanan, M. W., CO_2 Reduction at Low Overpotential on Cu Electrodes Resulting from the Reduction of Thick Cu_2O Films. J. Am. Chem. Soc. 134 (2012) 7231-7234.

(9) Raciti, D.; Livi, K. J.; Wang, C., Highly Dense Cu Nanowires for Low-Overpotential CO_2 Reduction. Nano Lett. 15 (2015) 6829-6835.

(10) Ma, M.; Djanashvili, K.; Smith, W. A., Controllable Hydrocarbon Formation from the Electrochemical Reduction of CO_2 over Cu Nanowire Arrays. Angew. Chem. Int. Ed. 55 (2016) 6680-6684.

(11) Sarfraz, S.; Garcia-Esparza, A. T.; Jedidi, A.; Cavallo, L.; Takanabe, K., Cu–Sn Bimetallic Catalyst for Selective Aqueous Electroreduction of CO_2 to CO. ACS Catal. 6 (2016) 2842-2851.

(12) Zhao, Y.; Wang, C.; Wallace, G. G., Tin Nanoparticles Decorated Copper Oxide Nanowires for Selective Electrochemical Reduction of Aqueous CO_2 to CO. J. Mater. Chem. A 4 (2016) 10710-10718.

(13) Huo, S.; Weng, Z.; Wu, Z.; Zhong, Y.; Wu, Y.; Fang, J.; Wang, H., Coupled Metal/Oxide Catalysts with Tunable Product Selectivity for Electrocatalytic CO_2 Reduction. ACS Appl. Mater. Interfaces 9 (2017) 28519-28526.

(14) Malik, K.; Singh, S.; Basu, S.; Verma, A., Electrochemical Reduction of CO_2 for Synthesis of Green Fuel. WIRES Energy Environ. 6 (2017) e244.

(15) Zhu, D. D.; Liu, J. L.; Qiao, S. Z., Recent Advances in Inorganic Heterogeneous Electrocatalysts for Reduction of Carbon Dioxide. Adv. Mater. 28 (2016) 3423-3452.

(16) Shih, C. F.; Zhang, T.; Li, J.; Bai, C., Powering the Future with Liquid Sunshine. Joule 2 (2018) 1925-1949.

(17) Yang, X. F.; Wang, A.; Qiao, B.; Li, J.; Liu, J.; Zhang, T., Single-Atom Catalysts: A New Frontier in Heterogeneous Catalysis. Acc. Chem. Res. 46 (2013) 1740-1748.

(18) Wang, A.; Li, J.; Zhang, T., Heterogeneous Single-Atom Catalysis. Nat. Rev. Chem. 2 (2018) 65-81.
(19) Zhang, Y. Zhang, Zeng, Z. Li, Hao. Design of 3d transition metal anchored B_5N_3 catalysts for electrochemical CO_2 reduction to methane. J. Mater. Chem. A 10 (2022) 9737-9745.
(20) Jiang, K.; Siahrostami, S.; Zheng, T.; Hu, Y.; Hwang, S.; Stavitski, E.; Peng, Y.; Dynes, J.; Gangisetty, M.; Su, D.; Attenkofer, K.; Wang, H., Isolated Ni Single Atoms in Graphene Nanosheets for High-Performance CO_2 Reduction. Energy Environ. Sci. 11 (2018) 893-903.
(21) Zhang, C.; Yang, S.; Wu, J.; Liu, M.; Yazdi, S.; Ren, M.; Sha, J.; Zhong, J.; Nie, K.; Jalilov, A. S.; Li, Z.; Li, H.; Yakobson, B. I.; Wu, Q.; Ringe, E.; Xu, H.; Ajayan, P. M.; Tour, J. M., Electrochemical CO_2 Reduction with Atomic Iron-Dispersed on Nitrogen-Doped Graphene. Adv. Energy Mater. 8 (2018) 1703487.
(22) Yang, H.; Wu, Y.; Li, G.; Lin, Q.; Hu, Q.; Zhang, Q.; Liu, J.; He, C., Scalable Production of Efficient Single-Atom Copper Decorated Carbon Membranes for CO_2 Electroreduction to Methanol. J. Am. Chem. Soc. 141 (2019) 12717-12723.
(23) Perdew, J. P.; Burke, K.; Ernzerhof, M., Generalized Gradient Approximation Made Simple. Phys. Rev. Lett. 77 (1996) 3865-3868.
(24) Blöchl, P. E., Projector Augmented-Wave Method. Phys. Rev. B 50 (1994) 17953-17979.
(25) Kresse, G., ab Initio Molecular Dynamics for Liquid Metals. J.Non-Crys. Solids 192 (1995) 222-229.
(26) Kresse, G.; Hafner, J., Ab Initio Molecular Dynamics for Open-Shell Transition Metals. Phys. Rev. B 48 (1993) 13115-13118.
(27) Peterson, A.A., Abild-Pedersen, F., Studt, F., Rossmeisl, J., Nørskov, J.K. How Copper Catalyzes the Electroreduction of Carbon Dioxide into Hydrocarbon Fuels. Energy Environ. Sci. 3 (2010) 1311-1315.
(28) Mathew, K.; Sundararaman, R.; Letchworth-Weaver, K.; Arias, T. A.; Hennig, R. G., Implicit solvation model for density-functional study of nanocrystal surfaces and reaction pathways. J. Chem. Phys. 140 (2014) 084106.
(29) Pei, S.; Cheng, H.-M., The Reduction of Graphene Oxide. Carbon 50 (2012) 3210-3228.
(30) Krasheninnikov, A. V.; Lehtinen, P. O.; Foster, A. S.; Pyykkö, P.; Nieminen, R. M., Embedding Transition-Metal Atoms in Graphene: Structure, Bonding, and Magnetism. Phys. Rev. Lett. 102 (2009) 126807.
(31) Cao, L.; Shao, Y.; Pan, H.; Lu, Z., Designing Efficient Dual-Metal Single-atom Electrocatalyst $TmZnN_6$ (Tm = Mn, Fe, Co, Ni, Cu, Zn) for Oxygen Reduction Reaction. J. Phys. Chem. C 124 (2020) 11301-11307.
(32) Rothenberg, G., Catalysis: Concepts and Green Applications, 2nd Edition (2017).
(33) Osouleddini, N.; Rastegar, S. F., DFT study of the CO2 and CH4 assisted adsorption on the surface of graphene. J Electron Spectros Relat Phenomena 232 (2019) 105-110.
(34) Zhao, S.; Xue, J.; Kang, W., Gas adsorption on MoS2 monolayer from first-principles calculations. Chem. Phys. Lett. 595-596 (2014), 35-42.
(35) Yang, J.; Johnson Goh, K. E.; Yu, Z. G.; Wong, R. E.; Zhang, Y. W., A first-principles study on strain engineering of monolayer stanene for enhanced catalysis of CO_2 reduction. Chemosphere 268 (2021) 129317
(36) Vollmer, S.; Witte, G.; Wöll, C., Determination of Site Specific Adsorption Energies of CO on Copper. Catal. Lett. 77 (2001) 97-101.

(37) Liu, X.; Xiao, J.; Peng, H.; Hong, X.; Chan, K.; Nørskov, J. K., Understanding Trends in Electrochemical Carbon Dioxide Reduction Rates. Nat. Commun. 8 (2017) 15438.
(38) Cheng, T.; Xiao, H.; Goddard, W. A., Full Atomistic Reaction Mechanism with Kinetics for CO Reduction on Cu(1 0 0) from ab Initio Molecular Dynamics Free-Energy Calculations at 298 K. Proc.Nati. Acad. Sci. 114 (2017) 1795-1800.
(39) Jiao, J.; Lin, R.; Liu, S.; Cheong, W. C.; Zhang, C.; Chen, Z.; Pan, Y.; Tang, J.; Wu, K.; Hung, S.-F.; Chen, H. M.; Zheng, L.; Lu, Q.; Yang, X.; Xu, B.; Xiao, H.; Li, J.; Wang, D.; Peng, Q.; Chen, C.; Li, Y., Copper atom-pair catalyst anchored on alloy nanowires for selective and efficient electrochemical reduction of CO_2. Nat. Chem. 11 (2019) 222-228.
(40) Peterson, A. A.; Nørskov, J. K., Activity Descriptors for CO_2 Electroreduction to Methane on Transition-Metal Catalysts. J. Phys. Chem. L 3 (2012) 251-258.